HHS Public Access

Author manuscript

Magn Reson Med. Author manuscript; available in PMC 2019 May 01.

Published in final edited form as:

Magn Reson Med. 2018 May ; 79(5): 2713–2723. doi:10.1002/mrm.26947.

Functional oxygen extraction fraction (OEF) imaging with turbo gradient spin echo QUIXOTIC (turbo QUIXOTIC)

Jeffrey N. Stout[1], **Elfar Adalsteinsson**[1,2], **Bruce R Rosen**[3,4], and **Divya S. Bolar**[2,3,5]

[1]Harvard-MIT Health Sciences and Technology, Institute of Medical Engineering & Science, MIT, Cambridge, MA, United States

[2]Department of Electrical Engineering and Computer Science, MIT, Cambridge, MA, United States

[3]Athinoula A. Martinos Center for Biomedical Imaging, Massachusetts General Hospital, MA, United States

[4]Department of Radiology, Harvard Medical School, Boston, MA, United States

[5]Department of Radiology, Massachusetts General Hospital, Boston, MA, United States

Abstract

Purpose—QUantitative Imaging of eXtraction of Oxygen and TIssue Consumption (QUIXOTIC) is a recent technique that measures voxel-wise oxygen extraction fraction (OEF), but suffers from long scan times limiting application. We implement multi-echo QUIXOTIC dubbed turbo QUIXOTIC (tQUIXOTIC) that reduces scan time by 8× and then apply it in functional MRI.

Methods—tQUIXOTIC utilizes a novel turbo gradient spin echo readout enabling measurement of venular blood transverse relaxation rate in a single tag-control acquisition. Using tQUIXOTIC we estimate cortical gray matter (GM) OEF, create voxel-by-voxel GM OEF maps, and quantify changes in visual cortex OEF during a blocked design flashing checkerboard visual stimulus. Contamination from CSF partial volume averaging is estimated and corrected.

Results—Average (N=8) cortical GM OEF was estimated as 0.38±0.06 using a 3.4 minute acquisition. Average OEF in the visual cortex was estimated as 0.43±0.04 at baseline and 0.35±0.05 during activation, with average %ΔOEF of -20%. These values are consistent with past studies.

Conclusion—tQUIXOTIC is introduced and shown to successfully estimate cortical GM OEF in clinical scan times and to detect changes in OEF during blocked design visual stimulation. tQUIXOTIC will be useful to monitor regional OEF clinically and in blocked design or event-related fMRI experiments.

Keywords

QUIXOTIC; oxygen extraction fraction; visual cortex; fMRI; quantification; blocked design; pulse sequence

Corresponding Author: Jeffrey N. Stout, jstout@mit.edu, (857) 919-1422, 77 Massachusetts Ave, Bldg 36-776A, Cambridge, MA 02139.

Introduction

Normal brain function depends on energy made available via cerebral oxygen metabolism. Oxygen extraction fraction (OEF) is directly related to the rate of cerebral oxygen metabolism ($CMRO_2$), and is a key quantitative indicator of brain function. As such, robust and reliable measurements of OEF have important clinical and basic neuroscience implications (1–3). Routine imaging of OEF, however, is not commonly performed in clinical or research settings, in part due to long acquisition times and complex protocols of typical MRI and PET approaches (4,5).

Clinically, OEF is relevant as an indicator of stroke risk (1) and a potential indicator of stroke ischemic penumbra, that is tissue at risk, but still viable (2). From a neuroscience standpoint, OEF offers a more direct assessment of metabolic changes than the traditional BOLD response, which is the mainstay of functional MRI (6,7). OEF reflects the balance of oxygen delivery and oxygen metabolism and is related to $CMRO_2$ by Fick's principle:

$$\mathrm{OEF}=\frac{\mathrm{CMRO_2}}{[\mathrm{Hb}]\cdot \mathrm{CBF}\cdot \mathrm{S_aO_2}} \quad [1]$$

where [Hb] is the blood concentration of hemoglobin, CBF is cerebral blood flow and S_aO_2 is the oxygen saturation of arterial blood (8,9). SaO_2 can be measured using a pulse oximeter, or in healthy adults assumed to be fully saturated.

There are three main classes of MRI-based techniques for quantifying regional cerebral OEF: magnetic susceptibility, T_2 relaxometry, and quantitative BOLD, reviewed in (3,4,10). These all measure OEF by quantifying effects of paramagnetic deoxygenated hemoglobin (dHb) in venous blood. T_2-relaxometry approaches are particularly appealing, as they typically offer less sensitivity to non-dHb sources of magnetic field inhomogeneity by eliminating extravascular signal. QUantitative Imaging of eXtraction of Oxygen and TIssue Consumption (QUIXOTIC) is among these intravascular T_2-relaxometry based approaches, in which T_2 of post-capillary venular blood is estimated and calibrated to venous oxygen saturation (SvO_2) and OEF (11–14).

The key innovation of QUIXOTIC is its ability to isolate signal from post-capillary venular blood on a voxel-wise basis, by using specialized velocity selective pulses that exploit differential blood velocities through the circulation (15). A two-step data acquisition paradigm is used where control and tag acquisitions are interleaved. In the control acquisition, a velocity selective module saturates all spins moving faster than some user defined cutoff velocity (V_{CUTOFF}). Blood spins are then allowed to decelerate into the capillary bed and accelerate into draining venules before being imaged some “outflow” time (TO) later. In the tag acquisition, after the first velocity selective module and outflow time, a second velocity selective module is used to saturate all blood spins that have accelerated into venules (faster than V_{CUTOFF}). Subtracting tag from control images generates an image where the signal primarily originates from blood in the post capillary venules.

A major limitation of QUIXOTIC is its long scan duration—only one echo time (TE) is acquired per repetition time (TR) and many repetitions are required to obtain enough SNR at the several echo times needed to determine T_2. The traditional QUIXOTIC approach therefore focused on acquiring one echo per scan, with each scan lasting several minutes. Standard single-run, blocked design functional MRI was not possible since T_2 (and thus OEF) could not be calculated every TR (16).

In this study, we have modified and improved the original QUIXOTIC approach (15) by implementing a turbo gradient spin echo (GRASE) (17) readout that acquires multiple echoes in a single TR, resulting in a several-fold decrease in imaging time, improved robustness to bulk motion and physiological noise, and providing the possibility to acquire a functional time series. We call this technique turbo QUIXOTIC (tQUIXOTIC). We demonstrate its effectiveness in estimating gray matter (GM) OEF in clinically feasible scan times, and then assess its ability to measure OEF changes in the visual cortex in response to a blocked design visual stimulus. We also estimate and correct for the effects of cerebrospinal fluid (CSF) diffusion attenuation on the tQUIXOTIC signal, a previously described confounder in the QUIXOTIC OEF measurement that is related to the application of velocity selective gradients intrinsic to the technique (15,18–20).

Methods

Construction of turbo QUIXOTIC sequence using a turbo gradient spin echo (GRASE) readout

To construct the tQUIXOTIC sequence, a custom GRASE readout utilizing adiabatic inversion pulses and spoiler gradients was added to the previously described QUIXOTIC pulse sequence (15) such that a complete set of control or tag images with different TEs is acquired in a single TR (Figure 1). This implementation of GRASE differs from the original (21) in that multiple images are generated per TR. We used a RF-pulse train with spoiler gradients for accurate and robust T_2 mapping (22). The spoiling gradients alternate in sign and linearly decrease in magnitude with every +/- pair. For improved robustness to B0 and B1 inhomogeneity, hyperbolic secant adiabatic pulses were implemented as the refocusing pulses. These pulses are nonselective, have a 3.142 ms duration, and are the same as those used in the velocity selective module (15,18). One complete echo planar imaging (EPI) readout is performed between each refocusing pulse and shortened to 12.6 ms using generalized autocalibrating partially parallel acquisitions (GRAPPA) parallel imaging technology (23), acceleration factor = 3. Notably, only even echoes from the GRASE readout were used for TE_1, TE_2, and TE_3 (as seen in Figure 1), as the odd echoes are contaminated by non-linear phase accrual from a single adiabatic inversion pulse, which is reversed after a pair (24). The accuracy of T_1 and T_2 quantification using the standalone GRASE module was verified using doped agar phantoms (3% Agar, 0.03 mM gadolinium) with similar T_1 and T_2 measurements to GM (15,25). The tQUIXOTIC sequence parameters used in the following experiments were V_{CUTOFF} = 2.3cm/s, TO_1 = 400 ms, outflow time (TO) = 725 ms, with GRASE readout parameters voxel size = 3.9×3.9×8 mm^3, FOV = 250 mm, $TE_1/TE_2/TE_3$/TR =25.2/50.4/75.6/3000 ms, BW = 3256 Hz/pixel.

Subject Selection and Data Acquisition

All scans of adult subjects took place at the Athinoula A. Martinos Imaging Center at the McGovern Institute for Brain Research, MIT. Eight healthy volunteers (aged 19 to 30, 4 males and 4 females) were scanned with IRB approval on a Siemens Tim Trio 3T scanner (Siemens Healthineers, Erlangen, Germany) using the Siemens 32-channel head coil.

The slice position for tQUIXOTIC imaging was chosen to intersect an area of the visual cortex that demonstrated a strong BOLD response to a visual stimulation paradigm. The calcarine fissure was located by visually inspecting a 1 mm^3 isotropic resolution three dimensional T_1-weighted, gradient echo structural scan (FOV = 256×256×176 mm^3 TE/TR = 3.44 / 2530 ms, GRAPPA acceleration factor = 3, total acquisition time = 4.3 min). An axial 2D slice selective EPI spin-echo (EPI-SE) scan that covered the primary visual cortex with seven slices was then acquired during a blocked design visual stimulus (8 Hz flashing radial checkerboard with central fixation point projected onto a translucent screen and viewed through a mirror mounted to the head coil) with one-minute periods of a central visual fixation point interleaved with one-minute periods of a central fixation point plus a radial checkerboard, for a total of five minutes (Figure 2). The EPI-SE scan parameters were: voxel size = 3.9×3.9×8 mm^3, FOV = 250 mm, TE/TR = 60/3000 ms, TR delay = 2385 ms, BW = 3256 Hz/pixel, scan time = 5 min. These data were analyzed by fitting a linear signal model consisting of regressors representing the blocked design stimulus, a linear and quadratic drift term, and a constant (DC) term. The slice showing the highest *t*-statistic values and largest volume of activation during the EPI-SE scan was selected for tQUIXOTIC imaging.

tQUIXOTIC imaging then took place in four 7-minute runs (4 minutes total at baseline and 3 minutes total during exposure to visual stimulus). During each run the aforementioned visual stimulus paradigm was displayed (Figure 2). After each tQUIXOTIC run, a double inversion recovery (DIR) image for GM-only imaging was acquired using the same slice position and spatial resolution. DIR imaging parameters were, TE/TR = 13/4340 ms, inversion times = 3700 ms and 4280 ms to select for GM only, 2232 Hz/Px bandwidth, and scan time = 6 s.

Turbo QUIXOTIC Analysis for OEF measurement in cortical GM and during visual stimulation

Analyses were performed using custom scripts for Neurolens (www.neurolens.org) and MATLAB (The Math Works, Natick, MA). Each tQUIXOTIC run was individually analyzed to determine OEF of cortical GM at baseline. Simple pairwise subtraction of tag and control images for corresponding TEs generated a tQUIXOTIC time series for each TE (TE_1, TE_2, and TE_3, Figure 2). Each series was smoothed with a 6 mm Gaussian kernel (26). The acquisitions during visual fixation only (excluding the 12 seconds following each period of stimulation, to allow OEF to return to baseline) were averaged across time to get a single baseline tQUIXOTIC image per TE. The corresponding DIR-GM image was used as a mask to select GM voxels within the baseline tQUIXOTIC images and the average GM signal intensity was calculated. For one subject, DIR images were not acquired; in this case the GM mask was generated by segmenting the EPI-SE images using FSL tools (BET and FAST) (27). These resulting tQUIXOTIC GM signal intensities were plotted against echo

time (TE_1, TE_2, and TE_3) and fit using the two-compartment signal model described below (Equation 3) using a non-linear least squares optimization method (MATLAB) to determine T_2 for venous blood in the cortical GM. T_2 values were then calibrated to venular blood oxygen saturation (SvO_2) based on empirical and biophysical models described in (11–14). This mapping depends on the hematocrit value for each subject, which we assumed to be the average standard values for hematocrit 0.45 for males and 0.42 for females (28), and on the inter-echo spacing of the GRASE train (12.6 ms). OEF for each state was then calculated as (SaO_2-SvO_2)/SaO_2, assuming fully saturated arterial blood in healthy adults (SaO_2 = 1).

Representative baseline OEF maps were generated for each tQUIXOTIC run for a single subject. As before, the baseline tQUIXOTIC data was pairwise subtracted, smoothed (10 mm Gaussian kernel) (15) and averaged across time, similar to the original QUIXOTIC mapping approach. On a voxel-wise basis, the tQUIXOTIC signal in cortical GM was again fit using the two-compartment signal model described below (Equation 3) to determine T_2 for venous blood in each voxel. SvO_2 and OEF were determined as above.

To determine OEF of a functionally activating region during both baseline and activation, the four tQUIXOTIC runs were averaged together. The average 7 min tQUIXOTIC run was then pairwise subtracted and smoothed (6 mm Gaussian kernel). For each TE, a linear signal model was fit to the 7-minute time series of each voxel. The linear signal model consisted of regressors representing the blocked design stimulus, a linear drift term, and a constant (DC). Maps of activation *t*-statistics were generated for each TE (Figure 3a). The *t*-statistic map for TE_3 was used to select a region of interest of the ten most significantly activating voxels (exceeding $P < 6.5\times10^{-4}$, corresponding to *t*-statistic > 3.35) excluding the region within 10 mm of the center of the superior sagittal sinus to avoid contamination from sinus venous blood. Beta-coefficients (β_{DC} and β_{EFFECT}) from the GLM fit were averaged over the region of interest. Fits of β_{DC} (baseline) and $\beta_{DC} + \beta_{EFFECT}$ (baseline plus effect size) for the three even echoes with the two-compartment signal model described below (Equations 2 and 3) determined T_2 values at baseline and during activation (Figure 3b).

T_2 Estimation and correction of CSF contamination to the tQUIXOTIC signal

Applying velocity selective gradients immediately before the imaging readout for the QUIXOTIC tag acquisition, but not during the control acquisition, results in a very small amount of diffusion weighting that is not eliminated upon control-tag subtraction (18). While this is negligible for most voxel constituents, a small component of CSF will persist and slightly contaminate the pure venular blood signal at longer echo times since $T_{2,CSF}$ is much longer than $T_{2,blood}$ (20). Assuming a two compartment model for blood and CSF in the voxel, the measured signal would be:

$$S(TE)=k_{blood}e^{-\frac{TE}{T_{2,blood}}}+k_{CSF}e^{-\frac{TE}{T_{2,CSF}}}. \quad [2]$$

Where, k_{CSF} and k_{blood} are the y-intercepts and $T_{2,CSF}$ and $T_{2,blood}$ are the transverse relaxation time constants for each compartment. Consequently, CSF signal contamination

creates an upward-bias in the estimated $T_{2,blood}$ when a monoexponetnial fit is used, which results in a lower estimated OEF.

Corrected values for baseline $T_{2,blood}$ and S_0 were determined by fitting a two compartment model, to the average tQUIXOTIC signal intensities, S(TE):

$$S(TE)=S_0\left[(1-X_{CSF})e^{-\frac{TE}{T_{2,blood}}}+(X_{CSF})e^{-\frac{TE}{T_{2,CSF}}}\right]. \quad [3]$$

X_{CSF} is the magnetization fraction of diffusion attenuated CSF in a GM voxel acquired with the specific tQUIXOTIC protocol that we used. X_{CSF} and $T_{2,CSF}$ were determined from calibration data from one subject through methods described in the appendix, and then used to correct the data for all other subjects. This assumes that that the volume fraction of CSF within GM voxels is relatively constant across humans, which is supported by several studies (29,30).

Since there is increased cerebral blood flow during neuronal activation X_{CSF} (fundamentally the ratio of diffusion attenuated CSF signal to blood signal) will change during activation. To account for this change, corrected values for $T_{2,blood}$ and k_{blood} during activation were determined by fitting Equation 2 to the average tQUIXOTIC signal intensities during stimulation, using $k_{CSF} = X_{CSF}*S_0$ and $T_{2,CSF}$ as determined from the corresponding baseline fitting. This approach reflects that CSF volume is assumed to remain constant during brain activation (29).

Results

Average cortical GM OEF at baseline for four runs from each subject are shown in Figure 4a, and values for T_2, SvO_2, and OEF are given in Table 1. The average T_2 for all subjects was 58±9 ms. Average SvO_2 was estimated as 62±6% and OEF as 0.38±0.06. Exponential fitting of the tQUIXOTIC signal averaged across GM voxels and over 3.4 minutes during baseline blocks, was high quality with $R^2 > 0.99$ for all fits. For OEF, the average coefficient of variation (COV) for all subjects across runs was 7%.

Representative OEF maps at baseline in GM are shown in Figure 5 for Subject 1. Average voxel-by-voxel OEF was 0.35±0.01 across the four maps, compared to 0.36±0.01 for the GM mask analysis.

During visual stimulation, significant changes in $T_{2,blood}$, SvO_2, and OEF were observed in the visual cortex. Results corrected for CSF contamination are given in Table 2. Figure 4b presents average cortical GM OEF at baseline, and OEF in the visual cortex at baseline and activation for each subject. Average baseline $T_{2,blood}$ was 50±6 ms and activation $T_{2,blood}$ was 64±8 ms. OEF changed (paired *t*-test, $P = 0.00001$) from 0.43±0.04 at baseline to 0.35±0.05 during activation with an average relative change of -20%. Exponential fitting of the tQUIXOTIC signal at baseline and activation averaged across ten voxels in the visual cortex was high quality with $R^2 > 0.99$ for all fits.

Data above is reported after correction for CSF contamination using $X_{CSF} = 0.112$, determined from calibration scans in cortical GM at 3.9×3.9×8 mm^3 resolution. Fit parameters for determining X_{CSF} as described in the appendix are given in Table 3. CSF correction did not alter the statistical significance of any reported comparisons. In cortical GM at baseline, uncorrected T_2 was on average 16±0.4 ms higher than corrected. Average uncorrected OEF was 0.29±0.05, or 0.09±0.01 lower than corrected OEF. X_{CSF} during activation—recalculated from k_{CSF} and k_{blood} after fitting—was 0.083±0.01 across all subjects.

Discussion

We have introduced a GRASE implementation of QUIXOTIC that permits estimation of regional cerebral oxygenation in a fraction of the original imaging time, making the technique feasible for clinical and functional imaging. The average estimate of baseline cortical GM OEF falls in the expected physiological range and is comparable to results from other MRI (9,26,31) and PET studies (32–34). We were able to demonstrate measurement of OEF in GM in 3.4 minutes, making tQUIXOTIC one of the fastest approaches for determining baseline OEF (4). It permits GM OEF mapping and was validated by performing a blocked design functional activation experiment using a flashing visual stimulus. Our results demonstrate a significant decrease in OEF during full field visual stimulation (average %ΔOEF = -20%, $P = 0.00001$) in agreement with previously reported values for OEF in visual activation paradigms (Table 4). To our knowledge, these results are the first MRI based measurements of regional OEF change with brain activation, based on a single functional time course, and without the use of external gases like oxygen or carbon dioxide. This becomes possible since tQUIXOTIC permits estimation of T_2 every two TR, since all echoes are acquired per TR.

tQUIXOTIC results without CSF correction are similar to the previously published QUIXOTIC results (see values in Table 4). Though QUIXOTIC scans are lengthy, baseline QUIXOTIC and tQUIXOTIC measurements of T_2 and OEF in cortical GM from one subject were acquired as a sanity check. Both scans were acquired from the same slice location, and GM was selected using a DIR scan as a mask. QUIXOTIC sequence parameters were as described in (15). For QUIXOTIC GM T_2 and OEF were 83±19 ms (mean ± standard error of the estimated parameter) and 0.25, respectively, and for tQUIXOTIC 77±3 ms and 0.28. These values are indistinguishable considering the standard errors, and fall within one standard deviation of the mean values for all subjects scanned with each technique. The standard errors given for both T_2 estimates underscore that though raw SNR over an imaging run is 2× lower using the GRASE readout in tQUIXOTIC, we observe improved fit quality in tQUIXOTIC (R^2>0.99) versus QUIXOTIC (R^2>0.95), which we attribute to the lower physiological noise and less bulk motion captured with tQUIXOTIC. tQUIXOTIC 8× faster overall, meaning that in terms of SNR per unit time tQUIXOTIC outperforms QUIXOTIC by 4×, which reduces the physiological noise during acquisition. Furthermore, by acquiring images from all TEs in every control and tag repetition there are far fewer periods were bulk motion can disrupt the tag-control difference images, and any motion should affect one repetition's images similarly.

Numerous PET and MRI studies find baseline OEF around 0.4 (34–37). Table 4 summarizes the OEF findings from other studies and supports the following comparisons. Without correcting for CSF contamination our estimates of cortical GM OEF values are in the lower MRI range (9,26,38), however after correction they are better agreement with both PET and MRI estimates (5,34–36,39,40), suggesting the CSF correction improves QUIXOTIC accuracy. Our standard deviation across subjects for cortical GM OEF of 0.06 is similar to the values reported by PET and MRI studies. Since tQUIXOTIC scans to determine OEF in GM at baseline required just a few minutes of data, we were able to perform multiple OEF measurements for each subject to ascertain intrasubject, same session, variability (Figure 4 and Table 1). The average same session COV, a metric of measurement noise, was 5.6% (discounting the large variation for subject 5 caused by a motion degraded run), which is slightly higher than the 3.2% reported for the whole-brain T_2-relaxation under spin tagging (TRUST) technique (37), even though TRUST benefits from high SNR in comparison to tQUIXOTIC. The intersubject COV, which in addition to measurement noise reflects the variance due to different physiology between subjects, was 15%. This is similar to that reported for other MRI techniques and corroborates the idea that baseline OEF is quite variable between subjects (41).

tQUIXOTIC is a voxel-by-voxel technique capable of producing cortical OEF maps in 3.4 minutes, as demonstrated in Figure 5. We observe that variation between maps from different runs is small, and that these maps appear qualitatively similar to those generated by qBOLD (35), and T_2 calibrated BOLD (36). It is reassuring that average OEF calculated for the voxel-by-voxel analysis and whole GM analysis were in excellent agreement. However, fits were generally not possible in white matter due to low SNR. Combining tQUIXOTIC runs was attempted to increase SNR, but suspected out-of-plane motion between runs and physiological noise (42) (over the course of 28 minutes of total scanning) diminished SNR gains despite the use of 2D-motion correction, and OEF mapping of white matter was not improved. Since tQUIXOTIC, as implemented, is a single slice technique with fairly low in-plane resolution (64×64 voxels in plane), out-of-plane motions are not well addressed by standard motion correction approaches. Future approaches will consider prospective motion correction strategies to improve SNR with longer acquisitions (43).

A robust response in the visual cortex to a flashing radial checkerboard stimulus makes it a popular paradigm for characterizing changes in cerebral oxygenation upon stimulation (9,11,26,40,44). We examined changes in OEF in the visual cortex due to visual stimulation to further validate tQUIXOTIC GM results and demonstrate the feasibility of tQUIXOTIC for detecting functional changes in brain state. The GRASE implementation is an important advance for functional imaging, as the required echoes for T_2 fitting and SvO_2 or OEF estimation are acquired in single tag-control acquisitions, giving a time point every two repetitions, which is similar to standard arterial spin labeling approaches that have been commonly used for functional challenges (6). This advance permits use of standard single-run, blocked and event-related functional paradigms, not possible with the original implementation. Whereas functional imaging with BOLD depends on blood volume, blood flow and tissue metabolism (7), and arterial spin labeling is only a marker of vascular changes (6), OEF-based functional imaging is related to the underlying balance between tissue metabolic demand and oxygen delivery. Ultimately, changes in $CMRO_2$, which could

be estimated by combining tQUIXOTIC derived OEF with a measure of local CBF (15), would permit direct quantitative assessment of cerebral metabolic demand. Further, given that baseline SvO_2 or OEF has been shown to modulate BOLD and CBF signal changes (39,41), fast approaches to OEF mapping may also provide useful calibration in multi-subject fMRI studies.

Our results for changes in OEF with visual stimulation are comparable to two previous calibrated BOLD studies at 3T (26) and (40), see Table 4. Our value for %ΔOEF is in excellent agreement with (26), -20% versus -21%, which used a similar visual stimulus (off 1 min, on 3 min, off 2 min). Notably our result for absolute OEF of 0.43 at baseline in the visual cortex is higher than that found in (26) of 0.29. Calibrated BOLD uses the information provided by hyperoxia and hypercapnia calibration experiments to determine baseline properties of the BOLD signal, which are then used to estimate absolute OEF and $CMRO_2$. In contrast, tQUIXOTIC is used to directly measure the T_2 from the venular blood compartment, which is empirically and theoretically related to SvO_2 (14). Thus, despite different modeling and dominant signal source (intravascular versus extravascular) the agreement between (26) and tQUIXOTIC for assessing relative change in OEF during activation in the visual cortex suggests both methods are sensitive to the same physiological change with stimulation when a similar stimulation paradigm is used. However, the different absolute OEF may be attributable to these underlying differences in methodology. Interestingly, the combined hyperoxia-hypercapnia calibrated BOLD technique found a higher baseline OEF of 0.435 at 7T (39), nearly identical to our value.

The other calibrated BOLD study, (40), found an absolute OEF at baseline in the visual cortex of 0.48, which is even higher than our own, but a much smaller %ΔOEF of -6.25% than observed in (26) or our own study. The authors of (40) attribute the small %ΔOEF to a decline in stimulus induced $CMRO_2$ over the long 20 min stimulation paradigm, which was necessary to present a graded gas challenge to calibrate the BOLD signal model used to calculate OEF and $CMRO_2$. These differences draw attention to the fact that the metabolic response to visual stimuli is still being investigated (45) and variations in the stimulus presentation such as visual field coverage, presentation duration and subject attention may also influence the OEF response.

We compared OEF in the visual cortex and in cortical GM for eight subjects (Figure 4b). In 6 subjects visual cortex OEF is higher than GM OEF (Figure 4b), which is a trend supported by MRI and PET studies (5,40). In two of the subjects the trend is reversed which is similar to that found in (26,46). Differences in the apparent distribution of OEF across the cortex could be explored with an upgraded tQUIXOTIC with improved SNR and multi-slice acquisition as we discus below, while a greater number of subjects would be needed to address the overall tendencies in OEF within the primary visual areas.

Our correction for signal contamination due to diffusion-attenuated CSF resulted in a greater change in $T_{2,blood}$ (-15.5 ms) than a previous study (-10.2 ms) that explored the contamination in the QUIXOTIC technique (20). Differences in sequence implementation that affect the degree of diffusion attenuation or the volume of the selected blood pool would directly impact the magnetization fraction, X_{CSF}, which could explain these different

changes in T_2. The approach of biexponential modeling to determine the signal contamination of CSF has been used previously (47). The signal contamination we determined is small given that the CSF volume fraction in a typical voxel (10.7% at baseline) is about double the blood volume (29). Most of the CSF signal is being eliminated during control-tag subtraction. In the healthy young adults who were subjects in our study, we are confident that our approach to CSF correction requires calibration scans only once per voxel size and QUIXOTIC parameter set, and the relevant correction factor can be applied to all similar scans. Differences in the CSF volume fractions between subjects has only a small effect on corrected OEF estimates (COV = ±3.4% and no bias, based on a Monte Carlo simulation using the 13% intersubject variation in CSF volume fraction reported in (30) as the expected variation in X_{CSF}) in comparison to the average same session variation we found (COV = 5.6%).

Many central nervous system pathologies that cause focal or regional oxygenation changes will not have significant fluctuations in CSF content, particularly in their early stages (e.g. early ischemic stroke). When detecting changes in OEF, non-CSF corrected tQUIXOTIC will certainly be useful in some cases, as the lesional OEF values can be compared to OEF in regions of normal brain. However, several central nervous system pathologies (e.g. Alzheimer's disease, certain brain tumors) and old age, can lead to different CSF to tissue volume ratios, in which case X_{CSF} might be a source of error in corrected OEF estimates. The proposed CSF correction addresses the volume fraction effect arising from single voxels (0.12 ml) deemed GM based on DIR scans. It is unclear how an overall change in CSF volume and brain volume affects the volume fraction of CSF in a nominally GM voxel of the size we use, since most studies investigating CSF volume fraction changes have been undertaken to correct the metabolite concentrations obtained from much larger (~8 ml) MR spectroscopy voxels, with one study suggesting no detectable change (48) while another shows larger intersubject variation that accompanies disease (49). Though higher resolution may minimize these fluctuations in CSF volume fraction, in specific settings like Alzheimer's disease, brain tumor, or studies of aging, we suggest that measuring X_{CSF} is important to ensure that estimates of OEF are not biased.

A two compartment exchange model was used to perform the T_2 to SvO_2 calibration (14,50), which depends on the subject's hematocrit and inter-echo spacing of the T_2 preparation module, with model coefficients empirically derived from T_2-relaxation under spin tagging (TRUST) data (14). TRUST varies TE based on pre-readout T_2 preparation, which is inherently insensitive to flow, in contrast to our GRASE approach, which will be slightly sensitive to flow effects. However, we assume that flow effects are minimal between the short 12.6 ms echoes, particularly given that most of the venular blood signal within the cortex is originating from low-velocity microvasculature. We acknowledge a small bias may exist since later echoes will have their corresponding signal intensity biased upward due to increased signal accumulation in venules. Experiments varying the inter-echo spacing will further characterize the magnitude of this error, although preliminary work in (15) suggests that this is a small source of error.

Additional work is also needed to characterize the tQUIXOTIC signal originating from larger vessels, such as the superior sagittal sinus, which limited the choice of activated visual

cortex voxels in this particular study. Theoretically, though tQUIXOTIC velocity selection should eliminate signal in large veins, turbulence and changes in flow direction when vessels emerge from the cortex and combine with larger veins may mean that some apparently slowly moving blood arrives in the superior sagittal sinus during TO. Similarly, signal appearing in the superior sagittal sinus in velocity selective arterial spin labeling experiments has been attributed to the nonmonotonic velocity of blood as it drains from the microvasculature into large vessels (51).

Future work on tQUIXOTIC will focus on improving the SNR of the technique and implementing a multi-slice readout. One approach to improve SNR will be to optimize the radio frequency pulse train in the GRASE module to reduce the signal intensity difference between odd and even echoes (52,53). Optimization will also reduce specific absorption ratio (SAR). Currently we operate tQUIXOTIC scans with the SAR limit set to IEC Level 1, and we were SAR limited to acquire only 6 echoes for the 7 minute tQUIXOTIC runs. We could further minimize SAR by empirically determining the lowest power necessary to meet the adiabatic threshold for the inversion pulses. tQUIXOTIC was implemented as a single slice technique such that one complete image could be acquired per TE and 6 second temporal resolution could be achieved overall. However, a multi-slice acquisition would significantly increase the value of tQUIXOTIC, in both clinical and functional settings, where regions of interest may not be known *a priori* and more regional measurements are desired. Specifically, improved volume coverage would permit exploration of how OEF is tied to neural activity, perhaps using retinotopic mapping to examine the specificity of BOLD in comparison to tQUIXOTIC based OEF. When a lower image-to-image temporal resolution is acceptable (for example in clinical and non-functional MRI applications), but multiple slice coverage is desired, the GRASE module could be substituted with a 3D segmented readout (e.g. 3D spiral or 3D GRASE) (54,55). For fMRI applications that still require high image-to-image temporal resolution, simultaneous multi-slice acquisition technology will allow acquisition of several slices per TR (56).

Conclusion

Turbo QUIXOTIC marks a 8× decrease in acquisition time over the original approach, enabling clinical and functional OEF imaging including cortical GM OEF mapping in 3.4 minutes and generation of an OEF time course for functional MRI. Future experiments will use tQUIXOTIC to quantify OEF changes during different challenges (e.g. gas inhalation and non-visual functional tasks), demonstrate $CMRO_2$ quantification with additional cerebral blood flow measurements, and evaluate OEF and $CMRO_2$ in pathology such as stroke and brain tumor.

Acknowledgments

This publication was made possible by grant number T90DA022759/R90DA023427 from the NIH Blueprint for Neuroscience Research and NIBIB-NIH grant 5T32EB1680. Divya Bolar is supported by an RSNA Research Resident/Fellow Grant.

Appendix

In the original QUIXOTIC technique (15), T_2 of blood is determined by fitting a monoexponetnial decay to the venular-blood weighted signal:

$$\mathrm{S(TE)}=k\mathrm{e}^{-\frac{\mathrm{TE}}{\mathrm{T_2}}}. \quad \text{[A1]}$$

However, due to diffusion weighting from the velocity selective module applied only for tag acquisitions, some CSF signal remains after control-tag subtraction (15,18). Thus, the T_2 of blood is overestimated by monoexponetnial fitting since the signal includes some portion of CSF with its much longer T_2.

One proposal for how to empirically correct this CSF signal contamination in QUIXOTIC (20), assumes that any QUIXOTIC signal remaining after a long TE (~400 ms) originates from CSF alone, since the T_2 of blood is considerably shorter than the T_2 of CSF and will have decayed into the noise. This CSF signal can then be subtracted from the QUIXOTIC signal to compensate for the CSF contamination at short TEs where the blood signal predominates:

$$S_{\mathrm{corrected}}(\mathrm{TE})=S_{\mathrm{uncorrected}}(\mathrm{TE})-k_{\mathrm{CSF}}\,e^{-\frac{\mathrm{TE}}{T_{2,\mathrm{CSF}}}} \quad \text{[A2]}$$

Since k_{CSF} is determined empirically by measuring the signal intensity from a second long TE image, this provides a simple empirical method to correct for CSF contamination in QUIXOTIC.

For tQUIXOTIC, we first attempted the approach described in (20), but increasing the number of refocusing pulses (from 6 to 32) at the nominal delta TE of 12.6 ms to reach TE = 400 ms was not possible due to SAR limits. We thus increased the ΔTE to acquire data at longer TEs, which utilized less refocusing pulses and was less SAR intensive.

We acquired calibration data from one subject to determine the appropriate CSF correction for a typical grey matter voxel and then applied this result to all our data acquired with the same resolution and acquisition parameters. The calibration data consisted of tQUIXOTIC acquisitions with different ΔTE values from one subject. ΔTE values were 12.6, 50, 60, 70, 80, 90 and 100 ms. Five echoes were acquired with each ΔTE, except for the standard three echoes for ΔTE = 12.6. The total scan duration was 317s per acquisition. A DIR image for GM-only imaging was collected after each acquisition using the parameters described previously.

Since the signal from CSF is purposefully suppressed by subtraction, we first determined the value of $T_{2,CSF}$ within GM using the pre-subtraction images. Images were smoothed and averaged over all grey matter. Each acquisition with different ΔTE was analyzed separately. Those acquisitions with two or more average signal intensities with TE ≥ 500 ms were then

fit assuming monoexponetnial decay (Equation A1), since all signal remaining at these long TEs should only be from CSF. These fits resulted in average $T_{2,CSF}$ = 1.2 s, which is similar to that computed in (20).

The calibration data was then analyzed using the same methods described for the tQUIXOTIC experiments. In short, the data was pairwise subtracted, smoothed (6 mm Gaussian kernel), and averaged across time. The corresponding DIR-GM image for each acquisition was used as a mask to select GM voxels and the average GM signal intensity was calculated.

We fit Equation 2, with $T_{2,CSF}$ = 1.2 s, to the average GM signal intensity and observed a large residual due to signal discontinuities when similar TEs were acquired with different ΔTE (Figure 6), suggesting that k_{CSF} and k_{blood} had some dependence on the inter-echo spacing (ΔTE) of the GRASE readout. We altered the Equation 2 model for the average signal intensity measured at each echo time (S(TE)) by introducing a linear dependence on ΔTE for both y-intercept terms:

$$S(\mathrm{TE}, \Delta\mathrm{TE}) = (x_1(\Delta\mathrm{TE}) + x_2)e^{-\mathrm{TE}/x_3} + (x_4(\Delta\mathrm{TE}) + x_5)e^{-\mathrm{TE}/1.2}. \quad [A3]$$

This data-driven alteration of the model dramatically improved fitting with an *F*-statistic = 133, $P < 5\times10^{-15}$. We suspect the variation in y-intercept with ΔTE is biophysical and may be due to exchange of water between voxel compartments or diffusion around high susceptibility veins in the CSF (8,57).

We then determined X_{CSF}, the magnetization fraction of diffusion attenuated CSF within a GM voxel, which is specific to the tQUIXOTIC parameters used in our experiments. Specifically, for ΔTE = 12.6 ms, $X_{CSF} = k_{CSF}/(k_{blood}+k_{CSF}) = 0.112$, where $k_{CSF} = x_4(0.0126)+x_5$ and $k_{blood} = x_1(0.0126)+x_2$ with x_i given in Table 3. The magnetization fraction (X_{CSF}) is valid for ΔTE = 12.6 - 100 ms, but X_{CSF} for ΔTEs > $0.5\cdot(T_{2,blood})$ are likely not relevant for tQUIXOTIC in practice, as the blood signal will have significantly decayed at these longer echo times. Variation in X_{CSF} for different ΔTE is due to the same biophysical properties hypothesized to affect the y-intercepts in Equation A3. To be clear, X_{CSF} is not the CSF volume fraction. It is the fraction of diffusion attenuated CSF that is not eliminated by control-tag subtraction in comparison to the venular-blood weighted signal resulting from QUIXOTIC velocity selection (i.e. the magnetization fraction). As long as the parameters of the velocity selective modules (i.e. the gradient, gradient pulse separation, and gradient pulse duration) are the same as what we used here, we would expect the same relative contribution of CSF contamination so this result could be applied to other studies. However, the approach of (20) is subject specific when used to correct QUIXOTIC acquisitions.

Corrected $T_{2.blood}$ values were then determined as described above, by fitting tQUIXOTIC data with the two-compartment model given in Equations 2 and 3.

References

1. Gupta A, Baradaran H, Schweitzer AD, Kamel H, Pandya A, Delgado D, Wright D, Hurtado-Rua S, Wang Y, Sanelli PC. Oxygen extraction fraction and stroke risk in patients with carotid stenosis or occlusion: A systematic review and meta-analysis. Am J Neuroradiol [Internet]. 2014; 35:250–255. DOI: 10.3174/ajnr.A3668
2. Heiss WD. Ischemic penumbra: evidence from functional imaging in man. J Cereb Blood Flow Metab. 2000; 20:1276–1293. DOI: 10.1097/00004647-200009000-00002 [PubMed: 10994849]
3. Christen T, Bolar DS, Zaharchuk G. Imaging Brain Oxygenation with MRI Using Blood Oxygenation Approaches: Methods, Validation, and Clinical Applications. AJNR Am J Neuroradiol [Internet]. 2012; :1–10. DOI: 10.3174/ajnr.A3070
4. Rodgers ZB, Detre JA, Wehrli FW. MRI-based methods for quantification of the cerebral metabolic rate of oxygen. J Cereb Blood Flow Metab [Internet]. 2016; doi: 10.1177/0271678X16643090
5. Ibaraki M, Miura S, Shimosegawa E, Sugawara S, Mizuta T, Ishikawa A, Amano M. Quantification of cerebral blood flow and oxygen metabolism with 3-dimensional PET and 15O: validation by comparison with 2-dimensional PET. J Nucl Med [Internet]. 2008; 49:50–9. DOI: 10.2967/jnumed.107.044008
6. Detre JA, Rao H, Wang DJJ, Chen YF, Wang Z. Applications of arterial spin labeled MRI in the brain. J Magn Reson Imaging. 2012; 35:1026–1037. DOI: 10.1002/jmri.23581 [PubMed: 22246782]
7. Buxton, RB. Introduction to Functional Magnetic Resonance Imaging: Principles and Techniques. Cambridge: Cambridge University Press; 2007.
8. van Zijl PCM, Eleff SM, Ulatowski JA, Oja JME, Ulug AM, Traystman RJ, Kauppinen RA. Quantitative assessment of blood flow, blood volue and blood oxygenation effects in functional magnetic resonance imaging. Nat Med. 1998; 4:159–167. [PubMed: 9461188]
9. Oja JM, Gillen JS, Kauppinen Ra, Kraut M, van Zijl PC. Determination of oxygen extraction ratios by magnetic resonance imaging. J Cereb Blood Flow Metab [Internet]. 1999; 19:1289–95. DOI: 10.1097/00004647-199912000-00001
10. Yablonskiy, Da, Sukstanskii, AL., He, X. Blood oxygenation level-dependent (BOLD)-based techniques for the quantification of brain hemodynamic and metabolic properties - theoretical models and experimental approaches. NMR Biomed. 2013; 26:963–986. DOI: 10.1002/nbm.2839 [PubMed: 22927123]
11. Golay X, Silvennoinen MJ, Zhou J, Clingman CS, Kauppinen Ra, Pekar JJ, van Zij PC. Measurement of tissue oxygen extraction ratios from venous blood T2: increased precision and validation of principle. Magn Reson Med [Internet]. 2001; 46:282–91.
12. Wright GA, Hu BS, Macovski A. 1991 I.I. Rabi Award. Estimating oxygen saturation of blood in vivo with MR imaging at 1.5 T. J Magn Reson Imaging [Internet]. 1991; 1:275–83.
13. Zhou J, Wilson Da, Ulatowski Ja, Traystman RJ, van Zijl PC. Two-compartment exchange model for perfusion quantification using arterial spin tagging. J Cereb Blood Flow Metab [Internet]. 2001; 21:440–55. DOI: 10.1097/00004647-200104000-00013
14. Lu H, Xu F, Grgac K, Liu P, Qin Q, van Zijl P. Calibration and validation of TRUST MRI for the estimation of cerebral blood oxygenation. Magn Reson Med [Internet]. 2012; 67:42–9. DOI: 10.1002/mrm.22970
15. Bolar DS, Rosen BR, Sorensen AG, Adalsteinsson E. QUantitative Imaging of eXtraction of Oxygen and TIssue Consumption (QUIXOTIC) Using Venular-Targeted Velocity- Selective Spin Labeling. Magn Reson Med [Internet]. 2011; 66:1550–1562. DOI: 10.1002/mrm.22946
16. Bolar DS, Sorensen AG, Rosen BR, Adlasteinsson E. Feasibility of QUantitative Imaging of eXtraction of Oxygen and TIssue Consumption (QUIXOTIC) to assess functional changes in venous oxygen saturation during visual stimulus. ISMRM. 2009; 17:3658.
17. Berstein, MA., King Kevin, K., Zhou, XJ. Handbook of MRI Pulse Sequences. Burlington, MA: Elsevier; 2004.
18. Wong EC, Cronin M, Wu WC, Inglis B, Frank LR, Liu TT. Velocity-selective arterial spin labeling. Magn Reson Med [Internet]. 2006; 55:1334–41. DOI: 10.1002/mrm.20906

19. Guo J, Wong EC. Venous oxygenation mapping using velocity-selective excitation and arterial nulling. Magn Reson Med [Internet]. 2012; 68:1458–71. DOI: 10.1002/mrm.24145
20. Guo J, Wong EC. Removal of CSF Contamination in VSASL and QUIXOTIC using a long TE CSF Scan. ISMRM. 2011; 19:2116.
21. Oshio K, Feinberg Da. GRASE (Gradient- and spin-echo) imaging: a novel fast MRI technique. Magn Reson Med. 1991; 20:344–349. DOI: 10.1002/mrm.1910200219 [PubMed: 1775061]
22. Poon CS, Henkelman RM. Practical T2 quantitation for clinical applications. J Magn Reson Imaging. 1992; 2:541–553. DOI: 10.1002/jmri.1880020512 [PubMed: 1392247]
23. Griswold MA, Jakob PM, Heidemann RM, Nittka M, Jellus V, Wang J, Kiefer B, Haase A. Generalized autocalibrating partially parallel acquisitions (GRAPPA). Magn Reson Med [Internet]. 2002; 47:1202–10. DOI: 10.1002/mrm.10171
24. Conolly S, Glover G, Nishimura D, Macovski a. A reduced power selective adiabatic spin-echo pulse sequence. Magn Reson Med [Internet]. 1991; 18:28–38.
25. Bolar, DS. Magnetic Resonance Imaging of the Cerebral Metabolic Rate of Oxygen Consumption (CMRO2). Massachusetts Institute of Technology; 2010.
26. Gauthier CJ, Desjardins-Crépeau L, Madjar C, Bherer L, Hoge RD. Absolute quantification of resting oxygen metabolism and metabolic reactivity during functional activation using QUO2 MRI. Neuroimage [Internet]. 2012; 63:1353–63. DOI: 10.1016/j.neuroimage.2012.07.065
27. Jenkinson M, Beckmann CF, Behrens TEJ, Woolrich MW, Smith SM. FSL. Neuroimage [Internet]. 2012; 62:782–90. DOI: 10.1016/j.neuroimage.2011.09.015
28. Wakeman L, Al-Ismail S, Benton a, Beddall a, Gibbs a, Hartnell S, Morris K, Munro R. Robust, routine haematology reference ranges for healthy adults. Int J Lab Hematol [Internet]. 2007; 29:279–83. DOI: 10.1111/j.1365-2257.2006.00883.x
29. Donahue MJ, Lu H, Jones CK, Edden RaE, Pekar JJ, Van Zijl PCM. Theoretical and experimental investigation of the VASO contrast mechanism. Magn Reson Med. 2006; 56:1261–1273. DOI: 10.1002/mrm.21072 [PubMed: 17075857]
30. Bender B, Klose U. Cerebrospinal fluid and interstitial fluid volume measurements in the human brain at 3T with EPI. Magn Reson Imaging [Internet]. 2009; 61:834–41. DOI: 10.1002/mrm.21915
31. Fan A, Evans KC, Stout JN, Rosen B, Adalsteinsson E. Regional Quantification of Cerebral Venous Oxygenation from MRI Susceptibility Mapping During Hypercapnia. Proc Intl Soc Mag Reson. 2014:752.
32. Leenders KL, Perani D, Lammertsma aa, Heather JD, Buckingham P, Healy MJ, Gibbs JM, Wise RJ, Hatazawa J, Herold S. Cerebral blood flow, blood volume and oxygen utilization. Normal values and effect of age. Brain [Internet]. 1990; 113(Pt 1):27–47.
33. Ibaraki M, Shinohara Y, Nakamura K, Miura S, Kinoshita F, Kinoshita T. Interindividual variations of cerebral blood flow, oxygen delivery, and metabolism in relation to hemoglobin concentration measured by positron emission tomography in humans. J Cereb Blood Flow Metab [Internet]. 2010; 30:1296–1305. DOI: 10.1038/jcbfm.2010.13
34. Ito H, Kanno I, Fukuda H. Human cerebral circulation: positron emission tomography studies. Ann Nucl Med [Internet]. 2005; 19:65–74. DOI: 10.1007/BF03027383
35. He X, Yablonskiy Da. Quantitative BOLD: mapping of human cerebral deoxygenated blood volume and oxygen extraction fraction: default state. Magn Reson Med [Internet]. 2007; 57:115–26. DOI: 10.1002/mrm.21108
36. An H, Lin W. Quantitative measurements of cerebral blood oxygen saturation using magnetic resonance imaging. J Cereb Blood Flow Metab [Internet]. 2000; 20:1225–36. DOI: 10.1097/00004647-200008000-00008
37. Liu P, Xu F, Lu H. Test-retest reproducibility of a rapid method to measure brain oxygen metabolism. Magn Reson Med [Internet]. 2013; 69:675–81. DOI: 10.1002/mrm.24295
38. Fan AP, Evans KC, Stout JN, Rosen BR, Adalsteinsson E. Regional quantification of cerebral venous oxygenation from MRI susceptibility during hypercapnia. Neuroimage [Internet]. 2014; 104:146–155. DOI: 10.1016/j.neuroimage.2014.09.068
39. Fan AP, Schäfer A, Huber L, Lampe L, von Smuda S, Möller HE, Villringer A, Gauthier CJ. Baseline oxygenation in the brain: Correlation between respiratory-calibration and susceptibility methods. Neuroimage [Internet]. 2016; 125:920–931. DOI: 10.1016/j.neuroimage.2015.11.007

40. Wise RG, Harris AD, Stone AJ, Murphy K. Measurement of OEF and absolute CMRO2: MRI-based methods using interleaved and combined hypercapnia and hyperoxia. Neuroimage [Internet]. 2013; 83:135–147. DOI: 10.1016/j.neuroimage.2013.06.008
41. Lu H, Zhao C, Ge Y, Lewis-Amezcua K. Baseline blood oxygenation modulates response amplitude: Physiologic basis for intersubject variations in functional MRI signals. Magn Reson Med [Internet]. 2008; 60:364–72. DOI: 10.1002/mrm.21686
42. Triantafyllou C, Polimeni JR, Wald LL. Physiological noise and signal-to-noise ratio in fMRI with multi-channel array coils. Neuroimage. 2011; 55:597–606. DOI: 10.1016/j.neuroimage.2010.11.084 [PubMed: 21167946]
43. Maclaren J, Herbst M, Speck O, Zaitsev M. Prospective motion correction in brain imaging: a review. Magn Reson Med [Internet]. 2013; 69:621–36. DOI: 10.1002/mrm.24314
44. Cheng Y, van Zijl PCM, Hua J. Measurement of parenchymal extravascular R 2 * and tissue oxygen extraction fraction using multi-echo vascular space occupancy MRI at 7 T. NMR Biomed [Internet]. 2015; 28:264–271. DOI: 10.1002/nbm.3250
45. Gagnon L, Smith AF, Boas DA, Devor A, Secomb TW, Sakadžić S. Modeling of Cerebral Oxygen Transport Based on In vivo Microscopic Imaging of Microvascular Network Structure, Blood Flow, and Oxygenation. Front Comput Neurosci [Internet]. 2016; 10:82.doi: 10.3389/fncom.2016.00082
46. Gauthier CJ, Hoge RD. Magnetic resonance imaging of resting OEF and CMRO 2 using a generalized calibration model for hypercapnia and hyperoxia. Neuroimage [Internet]. 2012; 60:1212–1225. DOI: 10.1016/j.neuroimage.2011.12.056
47. Brooks JC, Roberts N, Kemp GJ, Martin PA, Whitehouse GH. Magnetic resonance imaging-based compartmentation and its application\tto measuring metabolite concentrations in the frontal lobe. Magn Reson Med [Internet]. 1999; 41:883–888.
48. Huang W, Alexander GE, Chang L, Shetty HU, Krasuski JS, Rapoport SI, Schapiro MB. Brain metabolite concentration and dementia severity in Alzheimer's disease: a (1)H MRS study. Neurology [Internet]. 2001; 57:626–32.
49. Mato Abad V, Quirós A, García-Álvarez R, Loureiro JP, Alvarez-Linera J, Frank A, Hernández-Tamames JA. The Partial Volume Effect in the Quantification of 1H Magnetic Resonance Spectroscopy in Alzheimer's Disease and Aging. J Alzheimer's Dis [Internet]. 2014; 42:801–811. DOI: 10.3233/JAD-140582
50. Lu H, Ge Y. Quantitative evaluation of oxygenation in venous vessels using T2-Relaxation-Under-Spin-Tagging MRI. Magn Reson Med [Internet]. 2008; 60:357–63. DOI: 10.1002/mrm.21627
51. Wu WC, Wong EC. Intravascular effect in velocity-selective arterial spin labeling: The choice of inflow time and cutoff velocity. Neuroimage. 2006; 32:122–128. DOI: 10.1016/j.neuroimage.2006.03.001 [PubMed: 16713716]
52. Yetisir, F., Guerin, B., Poser, BA., Wald, LL., Elfar, A. ISMRM. Toronto, CA: 2015. Impact of RF-shimming on the uniformity and specific absorption rate of spin-echo imaging at 7 Tesla; p. 920
53. Guérin B, Gebhardt M, Cauley S, Adalsteinsson E, Wald LL. Local specific absorption rate (SAR), global SAR, transmitter power, and excitation accuracy trade-offs in low flip-angle parallel transmit pulse design. Magn Reson Med. 2014; 71:1446–1457. DOI: 10.1002/mrm.24800 [PubMed: 23776100]
54. Duhamel, G., Alsop, DC. ISMRM Anneual Meeting. 2004. Single-Shot Susceptibility Insensitive Whole Brain 3D fMRI with ASL; p. 518
55. Günther M, Oshio K, Feinberg DA. Single-shot 3D imaging techniques improve arterial spin labeling perfusion measurements. Magn Reson Med. 2005; 54:491–498. DOI: 10.1002/mrm.20580 [PubMed: 16032686]
56. Setsompop K, Gagoski BA, Polimeni JR, Witzel T, Wedeen VJ, Wald LL. Blipped-controlled aliasing in parallel imaging for simultaneous multislice echo planar imaging with reduced g-factor penalty. Magn Reson Med. 2012; 67:1210–1224. DOI: 10.1002/mrm.23097 [PubMed: 21858868]
57. Kandel, E., Schwartz, J., Jessell, T. Principles of Neural Science. New York: McGraw-Hill; 2000.

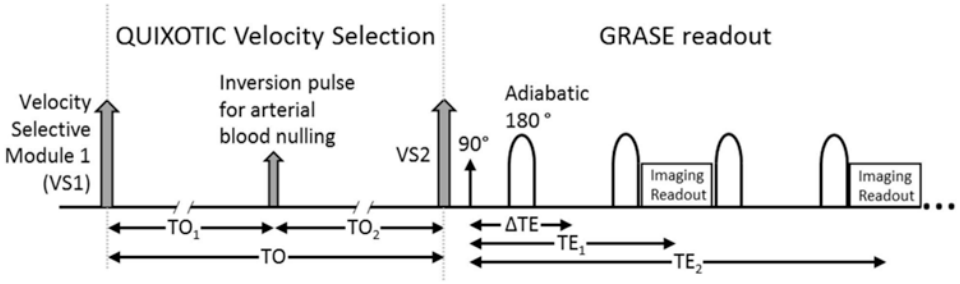

Figure 1.

Turbo QUIXOTIC Pulse Sequence. QUIXOTIC velocity selection followed by GRASE readout with one image acquired per TE.

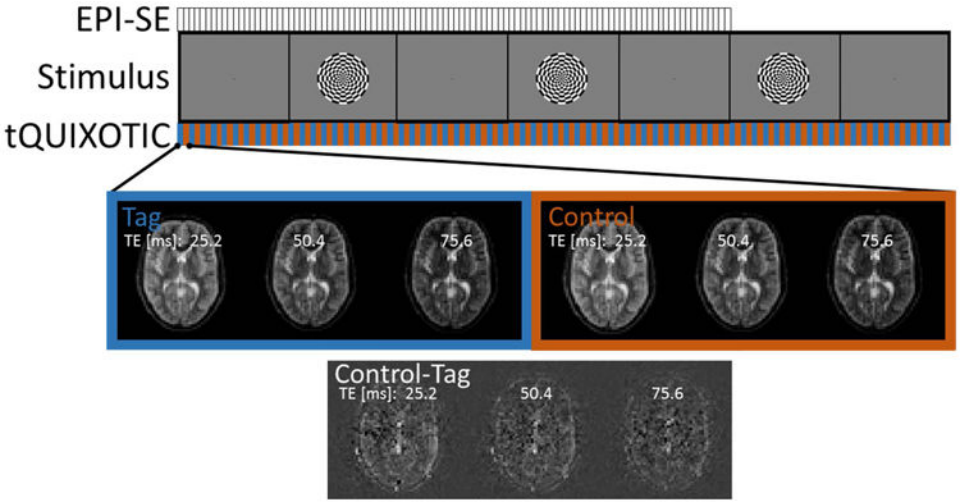

Figure 2.

Experimental Design. Visual stimulus paradigm of interleaved central visual fixation point (1 min) with flashing radial checkerboard (1 min), with total duration of 5 minutes for EPI-SE and 7 minutes for tQUIXOTIC. Example tQUIXOTIC tag or control image sets acquired for every TE in one TR = 3s.

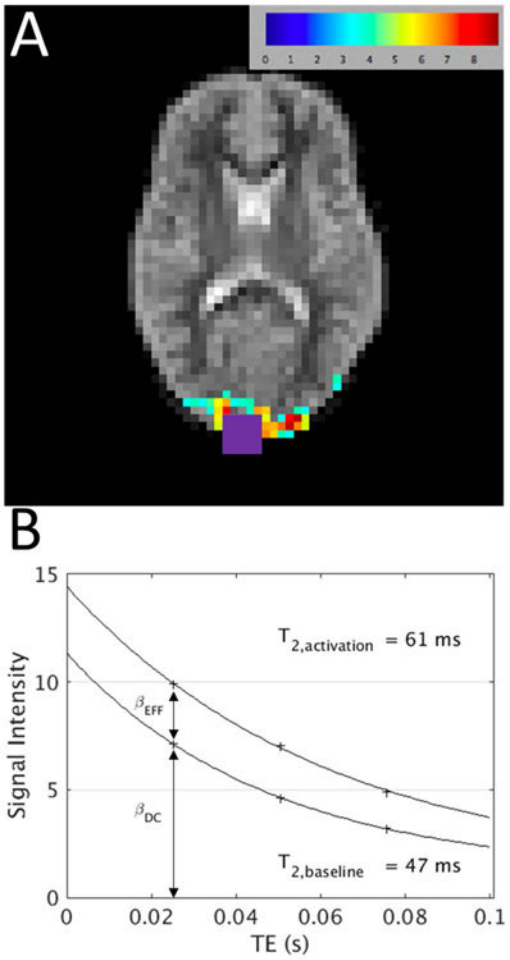

Figure 3.

Representative data analysis for subject 7. A) *t*-statistic map ($t > 3.4$) for the GLM fit of the TE_3 = 76.6 ms venular blood weighted image series overlaid on the first tag image (TE_1 = 25.2). SSS contaminated voxels determined from structural imaging are overlaid in purple and removed from further analysis. GLM regressors were stimulus convolved with hemodynamic response function (EFFECT), DC offset (DC) and linear drift. B) Corresponding plot of beta-coefficients from GLM (β_{DC} and (β_{DC} + β_{EFFECT}) from within activation ROI (10 voxels) versus TE, with T_2 fit lines.

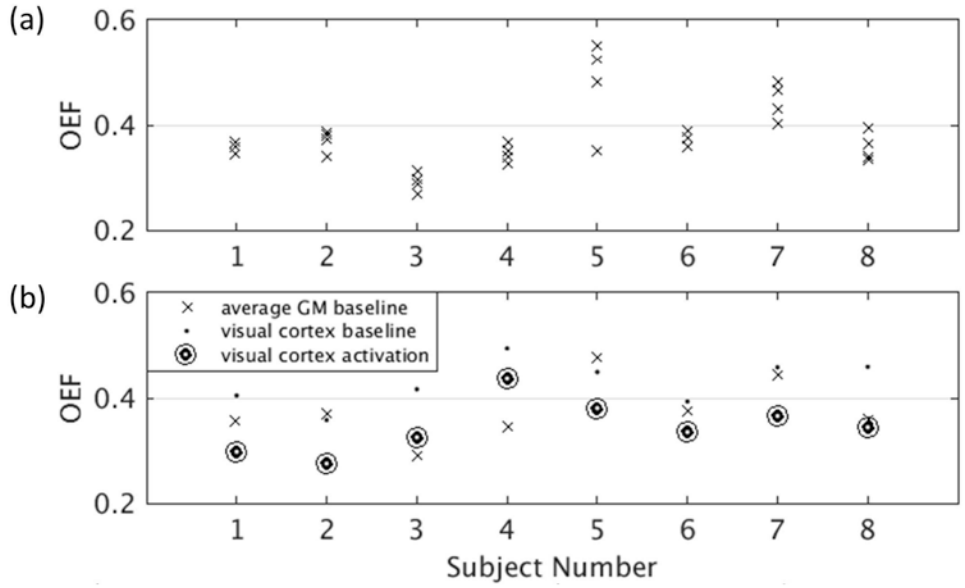

Figure 4.

(a) Average baseline GM OEF, corrected for CSF contamination, four runs for each subject, where a GM mask is used to average the tQUIXOTIC signal spatially before T_2 fitting. Baseline acquisition took 3.4 minutes per run. The average same session COV was 5.6%, not including the one motion degraded run for subject 5. (b) Average baseline GM OEF, baseline OEF in the visual cortex and activation OEF in the visual cortex, corrected for CSF contamination.

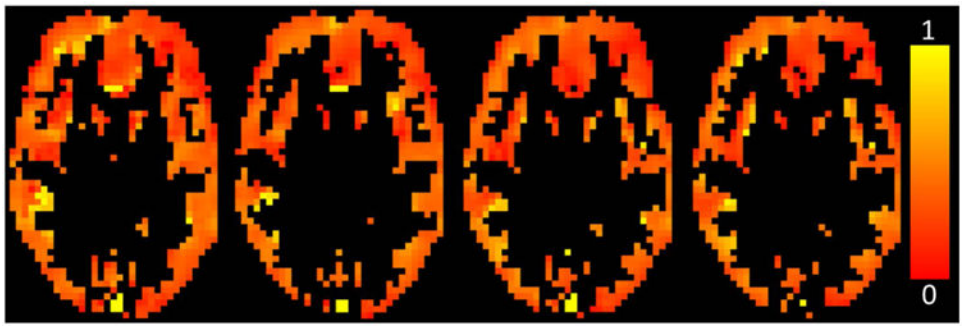

Figure 5.

OEF maps in the GM (determined by a separate DIR GM-selective scan) for each run of subject 1, after correction for CSF contamination, generated by fitting the tQUIXOTIC signal from each voxel.

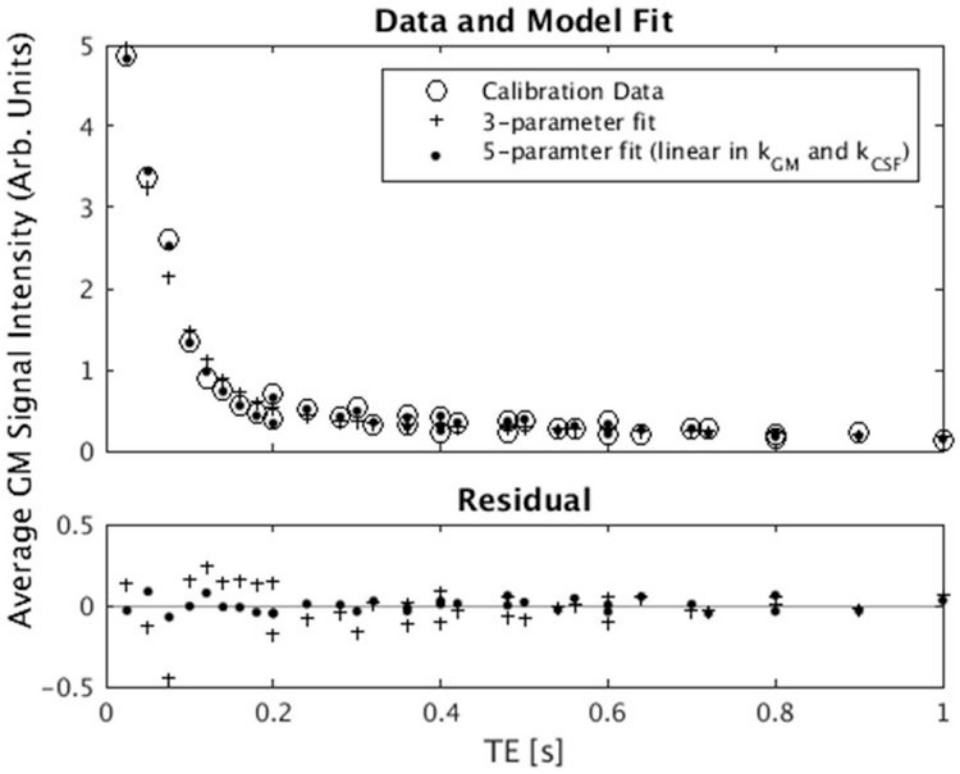

Figure 6.

Average GM signal intensity of the tQUIXOTIC calibration data for different ΔTE fitted with 3-parameter (Equation 2) and 5-parameter (Equation A3) models with $T_{2,CSF}$ = 1.2 s.

Table 1

Baseline GM T_2, SvO_2, and OEF for all subjects.

	T_2 [ms]						SvO_2 [%]						OEF					
Subject	**Run 1**	**Run 2**	**Run 3**	**Run 4**	**Mean**	**STD**	**Run 1**	**Run 2**	**Run 3**	**Run 4**	**Mean**	**STD**	**Run 1**	**Run 2**	**Run 3**	**Run 4**	**Mean**	**STD**
1	61	59	61	58	60	2	65	64	65	63	64	1	0.35	0.36	0.35	0.37	0.36	0.01
2	63	57	55	55	57	4	66	63	61	62	63	2	0.34	0.37	0.39	0.38	0.37	0.02
3	74	71	80	76	75	4	70	69	73	71	71	2	0.30	0.31	0.27	0.29	0.29	0.02
4	68	63	60	65	64	3	67	65	63	66	65	2	0.33	0.35	0.37	0.34	0.35	0.02
5	44	39	37	63	46	12	52	48	45	65	52	9	0.48	0.52	0.55	0.35	0.48	0.09
6	56	57	59	54	57	2	62	62	64	61	62	1	0.38	0.38	0.36	0.39	0.38	0.01
7	55	46	50	44	49	5	60	53	57	52	55	4	0.40	0.47	0.43	0.48	0.45	0.04
8	58	53	63	62	59	5	63	60	66	66	64	3	0.37	0.40	0.34	0.34	0.36	0.03
All Data					58±9						62±6						0.38±0.06	

Table 2

Baseline and activation T_2, SvO_2, and OEF values from the visual cortex showing a significant decrease in OEF with activation ($P = 0.00001$).

Subject	T_2 baseline [ms]	T_2 activation [ms]	ΔT_2 [ms]	SvO_2 baseline [%]	SvO_2 activation [%]	OEF baseline	OEF activation	%ΔOEF
1	52	71	18	60	70	0.40	0.30	-26
2	60	75	16	64	72	0.36	0.28	-23
3	53	68	16	58	67	0.42	0.33	-22
4	43	50	7	51	56	0.49	0.44	-12
5	48	58	10	55	62	0.45	0.38	-15
6	54	64	10	61	66	0.39	0.34	-15
7	47	61	14	54	63	0.46	0.37	-20
8	45	62	17	54	66	0.46	0.34	-25
Mean±STD	50±6	64±8	14±4.0	57±4	65±5	0.43±0.04	0.35±0.05	-20±5

Table 3

Fit parameters for model given in Equation A3, with $T_{2,CSF}$ = 1.2 s.

Model	**Residual sum of squares**	x_1	x_2	x_3	x_4	x_5
$(x_1(\Delta TE) + x_2)e^{-TE/x_3} + (x_4(\Delta TE) + x_5)e^{-TE/1.2}$	0.0511	-57.1	6.85	0.061	-4.88	0.835

Table 4

Baseline and activation OEF in published studies.

Study	Method	Baseline OEF	Activation OEF	Brain Region
Oja, et al. (1999). (9)	1.5T, T_2 mapping (N = 7)	0.3±0.06 *	0.2±0.07 *	Visual cortex
An and Lin, (2000). (36)	1.5T, multi-echo gradient and spin echo (N = 8)	0.416±0.018		Whole brain
He, et al., (2007). (35)	3T, quantitative BOLD (N = 9)	0.383±0.053		Whole brain
Cheng, et al. (2015). (44)	7T, VASO (N = 6)		0.24±0.01 *	Visual cortex
Fan, et al. (2014). (38)	3T, QSM (N = 10)	0.275±0.03 *		Occipital pial veins
Liu, et al. (2013). (37)	3T, TRUST (N = 7)	0.375±0.05		Whole brain
Guo, et al. (2012). (19)	3T, VSEAN (N = 4)	0.395±0.03		Gray matter
Bolar, et al. (2011). (15)	3T, QUIXOTIC (N = 10)	0.26±0.02		Gray matter
Ito, et al., (2005). (34)	PET (N = 70, multi-study review)	0.44±0.06		Whole brain
Ibaraki, et al. (2008). (5)	PET (N = 8)	0.40±0.06		Occipital cortex
		0.35±0.06		Gray matter
Gauthier, et al. (2012). (26)	3T, calibrated BOLD (QUO2) (N = 7)	0.29±0.05 *	0.23 ◊*	Visual cortex
Gauthier, et al. (2012). (46)	3T, calibrated BOLD (QUO2) (N = 8)	0.35±0.04		Gray matter
Fan, et al. (2016). (39)	7T, calibrated BOLD (QUO2) (N = 11)	0.435±0.14		Visual cortex
Wise, et al., (2013). (40)	3T, calibrated BOLD (N = 11)	0.48±0.09	0.45±0.14	Visual cortex
		0.42±0.12		Gray matter
This study	**3T, tQUIXOTIC (N = 8)**	**0.43±0.04**	**0.35±0.05**	**Visual cortex**
		0.38±0.06		**Gray matter**
		0.29±0.05		**GM, Not corrected for CSF**

◊ calculated from published results,

* different from comparable tQUIXOTIC result ($P < 0.05$))